Mechanical Peeling of Free-Standing Single-Walled Carbon-Nanotube Bundles

Changhong Ke, Meng Zheng, Guangwen Zhou, Weili Cui, Nicola Pugno, and Ronald N. Miles*

An in situ electron microscopy study is presented of adhesion interactions between single-walled carbon nanotubes (SWNTs) by mechanically peeling thin free-standing SWNT bundles using in situ nanomanipulation techniques inside a high-resolution scanning electron microscope. The in situ measurements clearly reveal the process of delaminating one SWNT bundle from its originally bound SWNT bundle in a controlled-displacement manner and capture the deformation curvature of the delaminated SWNT bundle during the peeling process. A theoretical model based on nonlinear elastica theory is employed to interpret the measured deformation curvatures of the SWNTs and to quantitatively evaluate the peeling force and the adhesion strength between bundled SWNTs. The estimated adhesion energy per unit length for each pair of neighboring tubes in the peeling interface based on our peeling experiments agrees reasonably well with the theoretical value. This in situ peeling technique provides a potential new method for separating bundled SWNTs without compromising their material properties. The combined peeling experiments and modeling presented in this paper will be very useful to the study of the adhesion interactions between SWNTs and their nonlinear mechanical behaviors in the large-displacement regime.

Keywords:
- adhesion
- carbon nanotubes
- delamination
- elastica

1. Introduction

Single-walled carbon nanotubes (SWNTs), a type of one-dimensional (1D) nanostructure, possess many extraordinary mechanical, electrical, thermal, and chemical properties,[1–8] and hold promise for many applications such as composites, electronics, and sensors.[9–11] Due to their high surface-to-volume ratio and the resulting strong adhesion interactions between SWNT surfaces, directly grown SWNTs are typically in the form of bundles instead of individual fibers. Understanding the adhesion between SWNTs is important not only to the separation of bundled SWNTs but also to applications where the adhesion plays an important role, such as carbon-nanotube-based nanoswitches[12,13] and nanotweezers.[14,15] The adhesion between SWNTs is due to van der Waals interactions between carbon atoms, which play a critical role at the nanoscale and dominate the intertube interactions between SWNTs. The adhesion between carbon nanotubes has been investigated by both modeling[16–21] and experiments.[13,22–24] Based on an atomistic/continuum model, Buehler et al. reported that individual high-aspect-ratio SWNTs can self-fold as a result of the balance between van der Waals forces and the bending force from the deformation of the SWNT.[16] Shortly thereafter, Zhou et al. reported a

[*] Dr. C.-H. Ke, M. Zheng, Dr. G.-W. Zhou, Dr. W.-L. Cui, Dr. R. N. Miles
Department of Mechanical Engineering
State University of New York at Binghamton
Binghamton, 13902 NY (USA)
E-mail: cke@binghamton.edu
Dr. N. Pugno
Department of Structural Engineering
Politecnico di Torino, Torino (Italy)

Supporting Information is available on the WWW under http://www.small-journal.com or from the author.

DOI: 10.1002/smll.200901807

NANO MICRO small

closed-form analytical solution predicting the contact length for self-folded single- and multi-walled carbon nanotubes.[20] Using a continuum model, Li et al. reported the nonlinear deformation of a SWNT above a SWNT-bundle substrate due to van der Waals forces.[17] Tang et al. reported, based on an atomistic/continuum model, the transverse deformation of the two SWNTs held together by van der Waals forces.[18] It is noted that in the aforementioned continuum and atomistic models, the calculations of the adhesion between SWNTs are based on perfect atomic structures of SWNTs. However, structural imperfections such as defects and surface contaminations, which are inevitably developed during the nanotube synthesis processes, may have a significant impact on the adhesion strength between nanotubes.[25,26] Therefore, experimental study of the adhesion between carbon nanotubes is imperative. The experimental work in the literature on quantitatively evaluating the intertube adhesion is quite limited, which is in part due to technical challenges associated with the nanoscale positioning and manipulation of nanostructures.[27] Bhushan et al. employed the atomic force microscopy (AFM) technique to study the adhesion and friction between a free-standing multi-walled carbon nanotube and a single-walled nanotube that is attached to the AFM probe as an extruding imaging tip.[22] When the AFM cantilever with the nanotube tip scans the free-standing nanotube in the tapping mode, the adhesion and friction interactions between these two nanotubes cause attenuation of the vibrational amplitude of the AFM cantilever, which can be used to estimate the adhesion and friction between nanotubes. Strus et al. investigated the adhesion interaction between multi-walled nanotubes and flat graphite substrates using a novel AFM-based peeling force spectroscopy technique.[23] In their experimental configuration, one individual nanotube was mounted on a tipless AFM cantilever as a cantilevered structure, which was first engaged to contact a graphite substrate and then peeled from the substrate by controlling the position of the AFM cantilever. The peeling force was measured by recording the deflection of the AFM cantilever when the nanotube was gradually peeled from the substrate. It is noted that, for both of the aforementioned experimental studies, the deformation curvatures of the tested nanotubes could not be measured directly due to the lack of a means of visualizing the nanotube during the experiments. Therefore, the evaluations of the adhesion energy in these studies have to rely purely on the postulated deformation curvature of the nanotubes.

In this Full Paper, we present an in situ electron microscopy study of the adhesion interactions between SWNTs by mechanically peeling thin free-standing SWNT bundles using in situ nanomanipulation techniques inside a high-resolution scanning electron microscope. Our in situ measurements clearly reveal the process of stripping off one SWNT bundle from its originally bound SWNT bundle in a controlled-displacement manner and capture the deformation curvature of the delaminated SWNT bundle during the peeling process. A theoretical model based on nonlinear elastica theory is employed to interpret the measured deformation curvatures of the SWNTs and to evaluate the peeling force and the adhesion energy between bundled SWNTs. The adhesion energy per unit length for each pair of neighboring tubes in the peeling interface is also quantitatively evaluated based on our peeling measurements and compared with the theoretical and experimental data reported in the literature.

2. Results and Discussion

2.1. In situ Peeling Experiments

The SWNTs employed in our study were originally grown on the surface of Si wafers in the form of high-density bundles by a chemical vapor deposition (CVD) method.[28] Transmission electron microscopy (TEM) copper grids (PELCO grids purchased from Ted Pella, Inc) were used to gently scratch the surface of the Si wafer with grown SWNTs on top. Some of the SWNTs were transported from the Si wafer to the copper grid in the form of thin free-standing bundles bridging the through-windows of the grid, as illustrated in Figure 1a. A

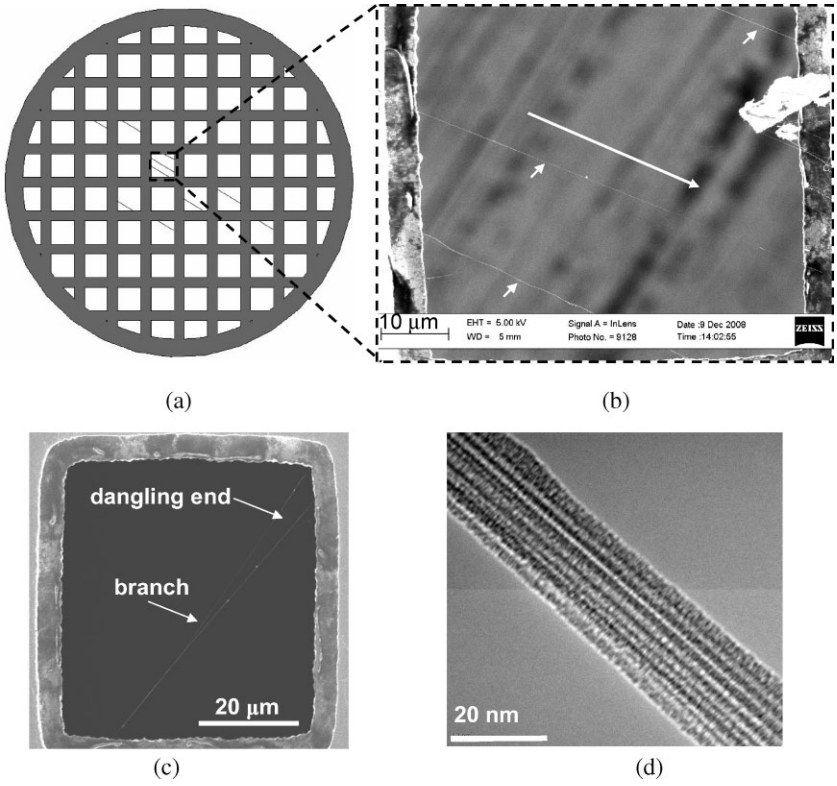

Figure 1. a) Schematic image of SWNT bundles bridging the through windows of a TEM copper grid. b) SEM image of one copper-grid window with three free-standing SWNT bundles across the edges of the grid through windows. c) SEM image of a free-standing SWNT bundle with a branch and a dangling end. d) HRTEM image of one free-standing SWNT bundle with a lateral dimension of 24 nm.

high-resolution scanning electron microscopy (HRSEM) system was used to inspect the grid and to identify the position and orientation of free-standing SWNT bundles on the grid. Our SEM imaging results reveal that the obtained free-standing SWNT bundles are consistently aligned parallel to the scratching direction. Figure 1b shows three free-standing SWNT bundles (small white arrows) across one grid through window, which are aligned along the scratching direction (large white arrow). Both ends of the free-standing SWNT bundles are attached to the grid surface by van der Waals interactions. Our studies show that about 20% of the obtained SWNT bundles ($n = 100$) have one or more branches and/or dangling ends, as exemplified by the SWNT bundle shown in Figure 1c. The dangling end is a small bunch of SWNTs, which is detached or loosely attached to other SWNTs in the same bundle. The free-standing SWNT bundles were inspected using a JEM 2100 high-resolution TEM (HRTEM) system operating at 200 kV and their lateral dimensions were measured with subnanometer resolution. The HRTEM images reveal that the SWNTs in the bundle are held together tightly by van der Waals forces and are aligned parallel to one another. Figure 1d shows a HRTEM image of a SWNT bundle with a lateral dimension of 24 nm. It is noted that information on the exact number of SWNTs and their assembly configuration in such bundles can not be measured readily by HRTEM imaging due to the overlapping effect. We would like to highlight that free-standing SWNT bundles can be obtained routinely using this scratching approach.

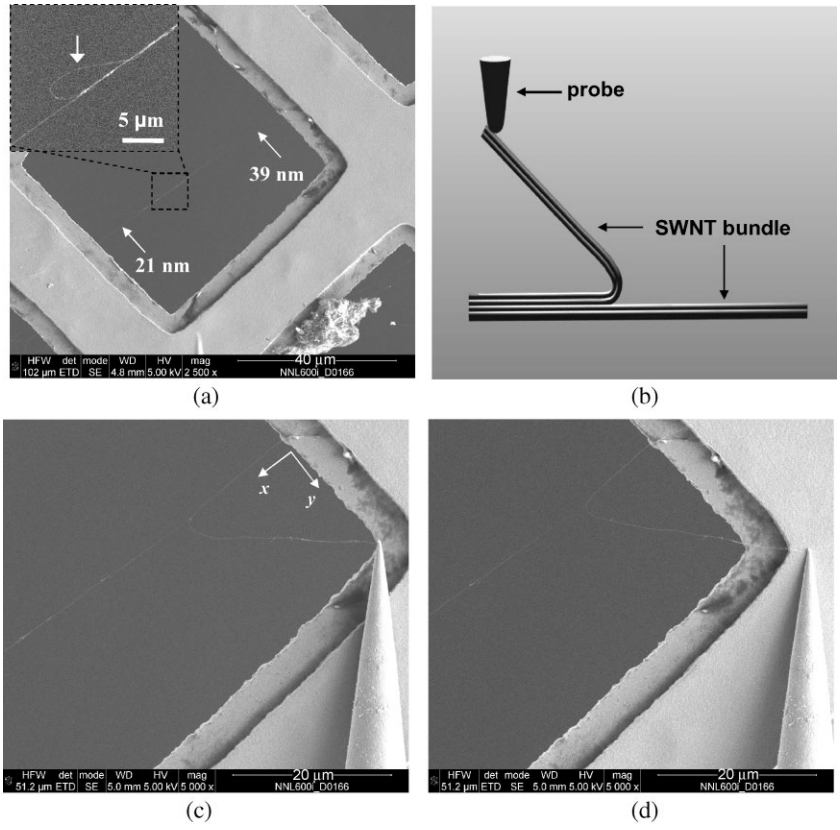

Figure 2. a) SEM image of a free-standing SWNT bundle with a dangling end (white arrow in the magnified inset). b) Schematic of the process of peeling off one SWNT bundle from its originally bound SWNT bundle by means of nanomanipulation. c,d) Two representative snapshots of peeling the SWNT bundle shown in (a) at two different peel-front positions.

Those free-standing SWNT bundles with branches and/or dangling ends can be used for peeling experiments in which one of the branching bundles or dangling ends is grabbed and then peeled off from its originally bound SWNT bundle. One representative peeling experiment is shown in Figure 2. Figure 2a show a SWNT bundle with a dangling end, which is clearly visualized in the magnified inset (white arrow) in Figure 2a. The length of the free-standing SWNT bundle between the two fixed ends is measured to be 56.5 μm. Because of the dangling end, one portion of the bundle has a larger lateral dimension than the other. The lateral dimensions of these two portions of the bundle were measured by HRTEM to be 39 and 21 nm, respectively (Figure S1 in the Supporting Information). A 3D piezo-driven nanomanipulator (Klocke Nanotechnik, Germany) mounted with a sharp tungsten probe was employed to perform in situ nanomanipulation inside the HRSEM.[29,30] The piezo stage of the nanomanipulator possesses nanometer-motion resolution in the x, y, and z directions. The motion and the position of the tungsten-probe tip can be visualized in real time by the electron beam. The in situ mechanical peeling experiment on the free-standing SWNT bundle is schematically illustrated in Figure 2b. When the manipulator probe was controlled to approach the dangling end of the SWNT bundle from the side, the dangling end jumped to make contact with the manipulator-probe tip due to van der Waals forces, and likely electrostatic forces, between the nanotubes and the probe. The manipulator probe was then controlled to move horizontally and to gradually peel the SWNT bundle whose dangling end is attached to the probe tip from its originally bound SWNT bundle, the ends of which are firmly attached to the surface of the copper grid. Each controlled peeling stroke produces a newly delaminated bundle with a length of ≈0.5–2.5 μm at a peeling speed of 1 or 2 μm s^{-1}. It is noted that no other fixture mechanism, such as electron-beam-induced hydrocarbon or Pt deposition,[29–31] was employed to strengthen the attachment of the end of the SWNT bundle to the tungsten probe. This observation suggests that the adhesion between carbon nanotubes and tungsten is stronger than that between the nanotubes themselves. In our experiments, the SWNT bundle and the manipulator-probe tip were controlled to be roughly at the same horizontal level by carefully adjusting the position and the orientation of the copper grid and controlling the position of the manipulator probe. The resulting deformation curvatures of the delaminated SWNT bundle during the peeling experiments stay practically in the horizontal plane and perpendicular to the electron beam.[32] Therefore, the deformation curvatures of the

NANO MICRO small

SWNT bundles can be measured with nanometer resolution by digitally analyzing the HRSEM images. Representative SEM snapshots of two different peeling stages of the same SWNT bundle shown in Figure 2a are presented in Figure 2c and d, respectively. The deformation curvature of the SWNT bundle at each delamination position is clearly captured by in situ SEM observation. The corresponding deformation behaviors are quantitatively measured from the SEM images and are presented later in Figure 4 as the circular- and square-dot curves, respectively. It should be emphasized that the delamination of the SWNT bundle and its deformation curvature are only attributed to the competition between the applied peeling force and the adhesion interactions between two SWNT bundles because the SWNT bundles employed in our peeling measurements are free-standing structures, thus excluding possible complications caused by other factors, such as the substrate effect, in the evaluation and modeling of the peeling force and the adhesion energy between SWNT bundles.

Using this in situ peeling technique, those bundled SWNTs that have dangling ends and/or branches can be physically separated with their material properties, such as surface chemical properties, untouched. This is in great contrast to many other SWNT-separation methods based on surface functionalization with surfactants[33] or biomolecules,[34] which usually compromise the surface properties of pristine SWNTs by introducing additional functional molecular groups to the surfaces of the SWNTs. Therefore, our in situ peeling technique provides a potential new method for separating bundled SWNTs while preserving their intact material properties, even though this debundling approach is, to some extent, time consuming and inefficient.

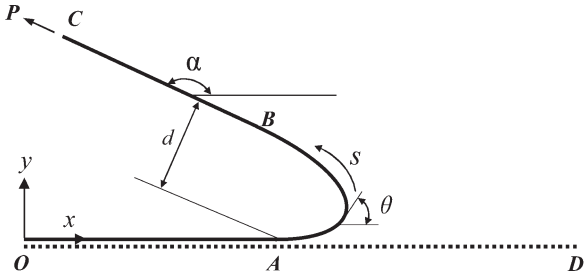

Figure 3. Schematic image of the theoretical model of SWNT-bundle-peeling experiments. The solid curve represents the delaminated SWNT bundle. The dotted curve represents the SWNT bundle with both ends fixed on the edges of the grid through window.

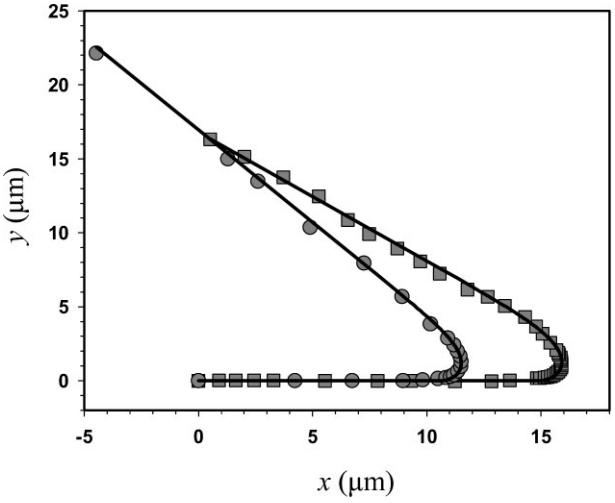

Figure 4. A comparison between the experimental measurements (dots) and theoretical predictions (solid line) of the deformation curves of the delaminated SWNT bundle shown in Figure 2c and d.

2.2. Modeling

As revealed by our in situ peeling experiments, the deformation of the delaminated SWNT bundle is clearly in the large-displacement regime, which is attributed to the ultrahigh mechanical strength and excellent flexibility of SWNTs. We model the delaminated SWNT bundle as an inextensible elastica rod,[35] which is consistent with the prior experimental observation that the nanotubes could be repeatedly bent to large angles and strain with no permanent distortion of the tube topography.[36] The simplified peeling configuration is schematically shown in Figure 3. The attachment of the SWNT bundle to the manipulator probe is considered as a joint connection based on the experimental observation. The deformation curve of the delaminated SWNT bundle ($OABC$) is divided into three regimes: segment OA, where two bundles are held together, and segments AB and BC. Point A is the delamination or peel-front point. Based on the inextensible elastica assumption, segment OA is considered to stay straight as well as the fixed–fixed SWNT bundle (segment OD in Figure 3), of which the deflection caused by the vertical component of the peeling force P is considered to be negligible. Segment AB is considered to be under pure bending and clamped at point A. Segment BC is considered to be under pure stretching by the peeling force P, implying that segment BC is a straight line with a slope angle of α and is tangential to segment AB at point B.

Our in situ peeling experiments are considered to be quasistatic processes, in which the deformation curvature of the delaminated bundle is determined by the bending moment generated by the peeling force. Here, the moment generated by the attractive van der Waals forces between segments ABC and AD is considered to be negligible. In the (s,θ) coordinate system, the governing equation of the deformed rod segment AB is given by

$$EI\frac{d^2\theta}{ds^2} - P\sin(\alpha-\theta) = 0, \quad (1)$$

where EI is the flexural rigidity of the rod and is assumed to be constant along the rod, s is the arc length along the deformed rod measured from the fixed end O, and θ is the angle between the tangent of the rod at s and the x axis. The boundary conditions at points A and B are $y_A = 0$, $\theta_A = 0$, $\theta_B = \alpha$, and $\frac{d\theta}{ds}|_B = 0$. In addition, it can be clearly seen that $\frac{d\theta}{ds} \geq 0$ for segment AB.

Following the approach reported in Reference [35], we obtain

$$\frac{d\theta}{ds} = \sqrt{\frac{2P}{EI}(1-\cos(\alpha-\theta))}. \quad (2)$$

Considering $dx = \cos\theta\, ds$ and $dy = \sin\theta\, ds$, the equation of segment AB is given by

$$x(\theta) = x_A + \beta \int_0^{\theta} \frac{\cos(\theta)d\theta}{\sqrt{1-\cos(\alpha-\theta)}} \quad 0 \le \theta \le \alpha \quad (3a)$$

and

$$y(\theta) = \beta \int_0^{\theta} \frac{\sin(\theta)d\theta}{\sqrt{1-\cos(\alpha-\theta)}} \quad 0 \le \theta \le \alpha \quad (3b)$$

where $\beta = \sqrt{\frac{EI}{2P}}$. β can be obtained by fitting the theoretically predicted deformation curve to the experimental data. The applied peeling force can be easily obtained as $P = \frac{EI}{2\beta^2}$, indicating that the applied peeling force is linearly proportionally to the bending stiffness of the delaminated bundle. The moment generated by P at point A, M_A, is given by $M_A = Pd$, in which d is the distance between point A and the acting line of the peeling force P.

Since our in situ peeling experiments are considered to be quasistatic processes, the delamination of the SWNT bundle is considered to be due to a balanced competition between the bending moment and the adhesion between SWNT bundles at the peel point. Therefore, the reaction moment at the peel point is equal to the bending moment measured in the vicinity of the peel point (i.e., M_A). Therefore, the adhesion energy per unit length or energy-release rate at the peel point is given by[37,38]

$$G = \frac{1}{2}\frac{M_A^2}{EI} = \frac{1}{8}\frac{EId^2}{\beta^4}. \quad (4)$$

We should emphasize that Equation (4) is valid for peeling in the large-displacement regime, as we present in our theoretical model, and can be also derived using a different approach with the same formulation. Nicholson demonstrated that the correlation between the peeling force P and the adhesion energy G, $G = P(1–\cos\alpha)$, is valid for peeling with both small and large bending.[39] Considering $d^2 = \frac{2EI}{P}(1-\cos\alpha)$, as derived by Kendall for a peel band with large displacements,[40] we can obtain the same formulation for the adhesion energy, G, as Equation (4).

The per-unit-area adhesion energy, which is generally used in the literature, can be easily obtained from Equation (4) provided that the width of the delaminated SWNT bundle at the peel point is known. Considering EI as a fundamental property of the SWNT bundle, as proposed by Huang et al. regarding the elastic behavior of SWNTs,[41–43] Equation (4) can be rewritten as $\frac{G}{EI} = \frac{1}{8}\frac{d^2}{\beta^4}$.

2.3. Comparison of Experiments and Theoretical Predictions

Figure 4 shows a comparison between the experimental measurements and the theoretical predictions of the two selected deformation curves of the delaminated SWNT bundle shown in Figure 2c and d. The theoretical predictions of the deformation of segment AB are obtained based on Equation (3), while the predicted segments OA and BC are obtained as the tangent lines to the predicted segment AB. Figure 4 clearly shows that the theoretical predictions and the experimental measurements are in good agreement for both deformation curves, with β as the only fitting parameter. In addition to β, the parameter d can be easily obtained from the theoretical curve by measuring the distance from point A to the extension line of segment BC, which coincides with the acting line of the peeling force P. Both the peeling force P and the adhesion energy G can then be obtained.

Figure 5a shows the applied peeling force, normalized by the flexural rigidity, EI, to delaminate the SWNT bundle shown in Figure 2a at different peel-front positions, which are determined based on ten recorded HRSEM images taken on

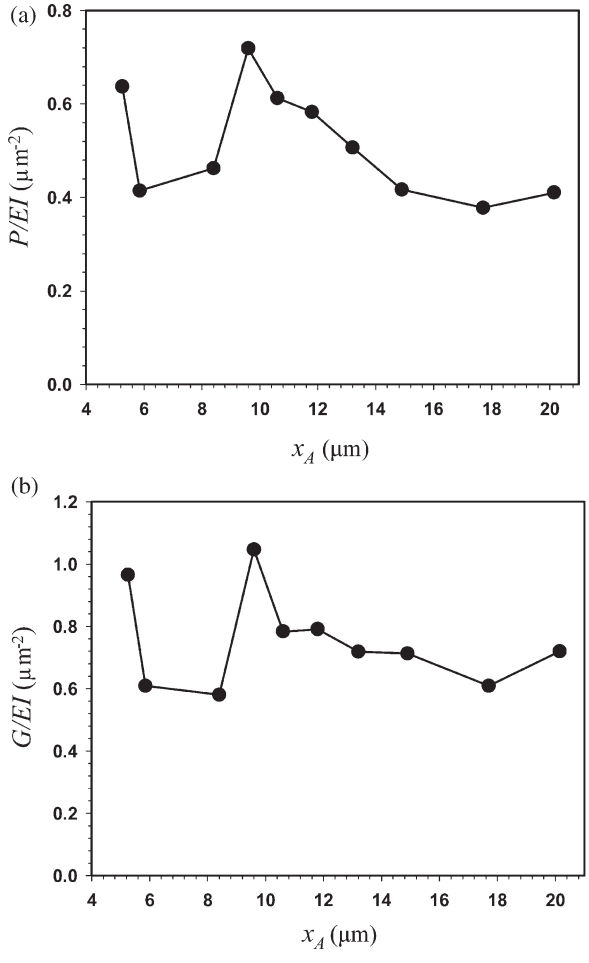

Figure 5. a) The predicted peeling force and b) the predicted adhesion energy per unit length between the SWNT bundles. Both the peeling force and the adhesion energy shown in the plots are normalized by EI.

NANO MICRO small

the same SWNT bundle at those respective peel-front positions. The corresponding theoretically predicted per-unit-length adhesion energy normalized by EI is plotted in Figure 5b. It can be seen from Figure 5b that the predicted adhesion energy fluctuates within a narrow range. Based on these ten measurements, the predicted adhesion energy $G = k\ EI$, in which $k = 0.75 \pm 0.15\ \mu m^{-2}$, represents a 20% variation from the mean value of the predicted adhesion energy. Such a variation in the adhesion energy may be attributed to several possible reasons. In addition to inaccuracies in theoretical modeling (e.g., the omission of the van der Waals interaction between segments ABC and AD in the current model), variations of SWNT structures at those peel-front points, such as defects and/or surface contamination, may also contribute to such fluctuations in the prediction of the adhesion energy.

It is noted that the first six data points, as counted from the left, in Figure 5a and b correspond to peeling measurements performed at a peeling speed of 1 $\mu m\ s^{-1}$, while the other four measurements were carried out at a peeling speed of 2 $\mu m\ s^{-1}$. Comparison of the predicted peeling force P and adhesion energy G for both peeling speeds suggests that the peeling speeds employed in our experiments do not have a material effect on the predicted peeling force and adhesion energy.

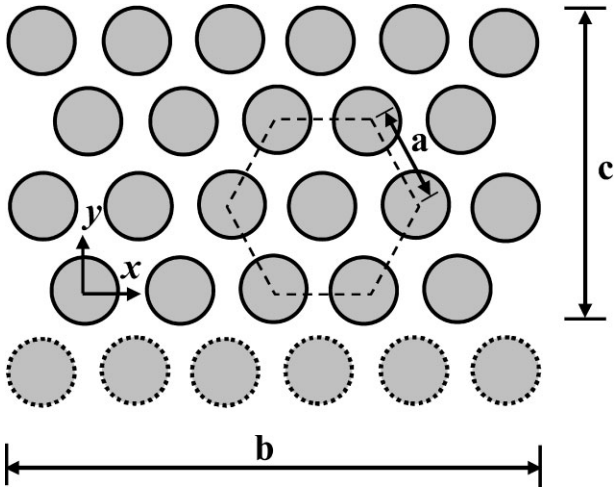

Figure 6. Schematic of the cross section of the SWNT bundles at the peel front. The dotted-circle rings represent the interface carbon nanotubes on the fixed bundle. The solid-circle rings represent carbon nanotubes on the delaminated bundle. a is the hexagonal lattice constant, b is the width of the delamination interface, and c is the height of the peeling cross section of the delaminated bundle.

2.4. Discussion of the Adhesion Energy Between Bundled SWNTs

Our theoretical model considers the bending stiffness EI to be a fundamental property of the delaminated SWNT bundle. The Young's modulus of individual SWNTs, E, is roughly 1 TPa.[44,45] Studies have shown that the Young's modulus of the SWNT bundles decreases as the tube diameter increases, which is due to the fact that the intertube van der Waals interaction is weaker than the nanotube's axial tensile strength which is attributed to covalent bonding.[46] The moment of inertia of the SWNT bundle, I, increases with the number of tubes in the bundle and also largely depends on their assembly configuration. On the other hand, the adhesion energy G can be considered to be linearly proportional to the number of tubes in the delamination interface because van der Waals interactions between non-neighboring carbon atoms are negligible.[47] Therefore, it is reasonable to speculate that the normalized adhesion energy, G/EI, is size dependent and decreases with an increase in the number of tubes in the bundle for the same tube assembly configuration. To facilitate a comparison of the adhesion energy between our experimental value and the available theoretical and experimental data in the literature, we calculate the adhesion energy per unit length between each pair of neighboring tubes in the peeling interface through a quantitative analysis of the dependences of G and EI on the cross-section dimensions of the bundle.

It has been reported previously that SWNTs in the bundle tend to form a orderly hexagonal structure,[48] as illustrated in Figure 6. Based on the HRTEM images of the tested samples, we assume that the delaminated SWNT bundle shown in Figure 2 consists of pure (10,10) SWNTs, which have a radius $r = 0.6785$ nm. The calculated Young's modulus for the (10,10) SWNT bundle is 0.563 TPa.[46] It is assumed that the radial deformation of the tubes in the bundle due to the intertube van der Waals interaction is negligible here[18] and that the cross sections of the tubes remain circular. The van der Waals interactions between carbon atoms are modeled by the Lennard-Jones (LJ) potential[49] as $u(R) = -\frac{A}{R^6} + \frac{B}{R^{12}}$, in which R is the atom-separation distance and A and B are constants (for carbon–carbon interactions, $A = 15.2$ eV Å^6 and $B = 24.1$ keV Å^{12}).[47] The equilibrium lattice constant for the bundled tubes, which corresponds to the minimum total van der Waals energy, can be estimated as $a = 2r + 0.313$ nm,[47] which gives $a = 1.67$ nm for (10,10) tubes. The corresponding van der Waals energy per unit length between two neighboring tubes in the peeling interface is given by[47] $G_0^{Theo} = \frac{3\pi n_\sigma^2}{8r^3}(-AI_A + \frac{21B}{32r^6}I_B)$, in which $n_\sigma = 38\ nm^{-2}$ is the graphene surface density and I_A and I_B are two double integrals and functions of a/r. For the parameters discussed here, the adhesion energy G_0^{Theo} is 0.151 nJ m^{-1}, which was originally reported in Reference [47]. The moment of inertia of the delaminated bundle is given by $I = NI_0 + A_0 \sum (y_i - y_c)^2$, in which N is the total number of tubes in the bundle, A_0 and I_0 are the cross-sectional area and moment of inertia of the individual SWNTs, calculated as $A_0 = \pi r^2$ and $I_0 = \pi r^4/4$, respectively, and y_i and y_c are the y coordinate of the center of each carbon nanotube and the centroid of the cross-section of the delaminated bundle, respectively. Based on the measured value of the height of the delaminated bundle (c in Figure 6), 18 nm, we reasonably assume that there are 13 layers of (10,10) tubes in the height direction of the delaminated bundle, which gives an actual height of 18.71 nm. Because the width of the delaminated bundle, b, is unknown, we calculated the adhesion energy per unit length between two neighboring tubes on the peeling interface, G_0, for a wide range of values of b from 3.03 to 49.79 nm, based on the experimental value of G/EI. The results are plotted in Figure 7. Figure 7 also show a 20% error bar

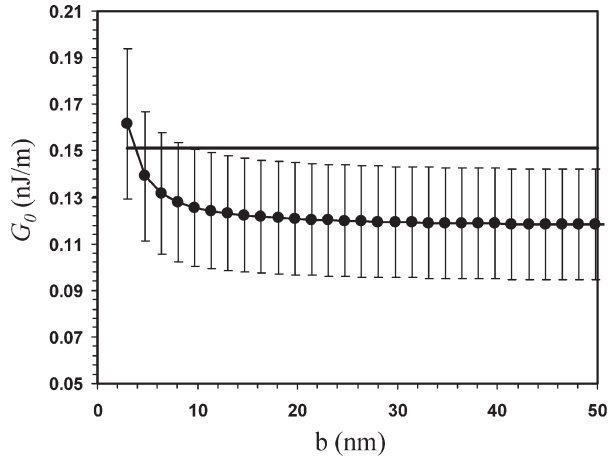

Figure 7. The dotted line and error bars represent the predicted mean value of the adhesion energy per unit length between two neighboring tubes on the peeling interface and its upper/lower limits for various delaminated SWNT bundle widths (*b*), respectively, based on the experimental value of *G/EI*. The solid line represents the theoretical prediction based on perfect SWNT-bundle structures.

indicating the upper/lower limit of the predicted adhesion energy for the tested bundle and a comparison with the theoretical value based on perfect SWNT-bundle structures. Our results show that the predicted adhesion energy decreases with increase of b and then tends to a constant value, which is ascribed to the edge effect. Figure 7 also shows that the theoretical value falls between the calculated mean and its upper/lower limits for our tested sample for $b \leq 9.707$ nm, implying that it is very likely that there are at most 5 layers of tubes in the width direction of the delaminated bundle. For b between 3.027 and 9.707 nm, the calculated mean value of the adhesion energy for our tested bundle is in the range of $\approx$0.126–0.162 nJ m^{-1}, which is close to the theoretical value for perfect SWNT bundles, and the difference increases with b. For instance, the difference is 7.7% for $b = 4.697$ nm and increases to 16.6% for $b = 9.707$ nm. Considering the possible structural imperfections in our tested bundle, the adhesion energy between SWNTs obtained from our peeling experiments agree reasonably well with the theoretical value and the tube-assembly configuration employed in our analysis appears to be plausible.

It is noted that the experimental values of the adhesion energy between two carbon nanotubes reported in the literature are in the range of $\approx$0.36–1.0 nJ m^{-1},[22,24] which were obtained based on the interactions between two double-walled nanotubes,[24] and between one single- and one multi-walled nanotube.[22] Our experimental value for SWNTs is smaller than those reported values, which is of no surprise because, in those systems, more carbon atoms were involved in the intertube interactions and the adhesion energy should be stronger compared to our pure-SWNT systems. We would like to highlight that, due to the fact that our peeling experiments can record the adhesion interaction between SWNTs at various locations on the same SWNT bundle, the adhesion energy estimated from our measurements will be statistically more reliable than those obtained based on measurements on just one location.[24]

3. Conclusion

In this Full Paper, we study the adhesion interactions between SWNTs by mechanically peeling thin free-standing SWNT bundles using in situ nanomanipulation techniques inside a HRSEM system. Our in situ measurements clearly capture the SWNT-bundle-delamination process. Theoretical predictions of the deformation curves of the delaminated SWNT bundles based on a nonlinear-elastica model are in good agreement with experimental measurements. The peeling force and the adhesion energy between bundled SWNTs are also quantitatively evaluated and discussed. The estimated adhesion energy per unit length for each pair of neighboring tubes in the peeling interface based on our peeling experiments agrees reasonably well with the theoretical value. Our in situ peeling technique provides a potential new method for separating bundled SWNTs without compromising their material properties. The combined peeling experiments and modeling presented in this paper will be very useful to the study of the adhesion interactions between SWNTs and their nonlinear mechanical behaviors in the large-displacement regime.

Acknowledgements

This work was supported by the State University of New York at Binghamton. The nanomanipulation measurements were performed using the facilities in the Analytical and Diagnostics Laboratory at Binghamton University's Small Scale Systems Integration and Packaging Center (S^{3}IP). The authors thank Dr. D. C. Sun for many helpful discussions.

[1] M. S. Dresselhaus, G. Dresselaus, P. Avouris, *Carbon Nanotubes*, Springer, Berlin **2001**.
[2] J. Y. Huang, S. Chen, Z. Q. Wang, K. Kempa, Y. M. Wang, S. H. Jo, G. Chen, M. S. Dresselhaus, Z. F. Ren, *Nature* **2006**, *439*, 281.
[3] D. Qian, G. J. Wagner, W. K. Liu, M. F. Yu, R. S. Ruoff, *Appl. Mech. Rev.* **2002**, *55*, 495.
[4] B. Liu, H. Jiang, H. T. Johnson, Y. Huang, *J. Mech. Phys. Solids* **2004**, *52*, 1.
[5] T. Lin, V. Bajpai, T. Ji, L. M. Dai, *Aust. J. Chem.* **2003**, *56*, 635.
[6] H. Jiang, B. Liu, Y. Huang, K. C. Hwang, *J. Eng. Mater. Technol.* **2004**, *126*, 265.
[7] J. Hone, M. C. Llaguno, M. J. Biercuk, A. T. Johnson, B. Batlogg, Z. Benes, J. E. Fischer, *Appl. Phys. A* **2002**, *74*, 339.
[8] D. Tasis, N. Tagmatarchis, A. Bianco, M. Prato, *Chem. Rev.* **2006**, *106*, 1105.
[9] H. G. Craighead, *Science* **2000**, *290*, 1532.
[10] B. Mahar, C. Laslau, R. Yip, Y. Sun, *IEEE Sensors J.* **2007**, *7*, 266.
[11] J. N. Coleman, U. Khan, Y. K. Gun'ko, *Adv. Mater.* **2006**, *18*, 689.
[12] T. Rueckes, K. Kim, E. Joselevich, G. Y. Tseng, C. L. Cheung, C. M. Lieber, *Science* **2000**, *289*, 94.
[13] J. Cumings, A. Zettl, *Science* **2000**, *289*, 602.
[14] S. Akita, Y. Nakayama, S. Mizooka, Y. Takano, T. Okawa, Y. Miyatake, S. Yamanaka, M. Tsuji, T. Nosaka, *Appl. Phys. Lett.* **2001**, *79*, 1691.
[15] P. Kim, C. M. Lieber, *Science* **1999**, *286*, 2148.

[16] M. J. Buehler, Y. Kong, H. Gao, Y. Huang, *J. Eng. Mater. Technol.* **2006**, *128*, 3.
[17] Z. L. Li, P. Dharap, S. Nagarajaiah, R. P. Nordgren, B. Yakobson, *Int. J. Sol. Struct.* **2004**, *41*, 6925.
[18] T. Tang, A. Jagota, C. Y. Hui, *J. Appl. Phys.* **2005**, *97*, 074304.
[19] W. Zhou, Y. Huang, B. Liu, J. Wu, K. C. Hwang, B. Q. Wei, *Nano* **2007**, *2*, 175.
[20] W. Zhou, Y. Huang, B. Liu, K. C. Hwang, J. M. Zuo, M. J. Buehler, H. Gao, *Appl. Phys. Lett.* **2007**, *90*, 073107.
[21] M. J. Buehler, *J. Mater. Res.* **2006**, *21*, 2855.
[22] B. Bhushan, X. Ling, A. Jungen, C. Hierold, *Phys. Rev. B* **2008**, *77*, 165428.
[23] M. C. Strus, L. Zalamea, A. Raman, R. B. Pipes, C. V. Nguyen, E. A. Stach, *Nano Lett.* **2008**, *8*, 544.
[24] B. Chen, M. Gao, J. M. Zuo, S. Qu, B. Liu, Y. Huang, *Appl. Phys. Lett.* **2003**, *83*, 3570.
[25] K. Kendall, *Molecular Adhesion and its Applications*, Kluwe Academic/Plenum Publishers, New York **2001**.
[26] B. Bhushan, *Philos. Trans. R. Soc. A* **2008**, *366*, 1499.
[27] Y. Zhu, C. Ke, H. D. Espinosa, *Exp. Mech.* **2007**, *47*, 7.
[28] W. Z. Li, S. S. Xie, L. X. Qian, B. H. Chang, B. S. Zou, W. Y. Zhou, R. A. Zhao, G. Wang, *Science* **1996**, *274*, 1701.
[29] C. H. Ke, H. D. Espinosa, *Small* **2006**, *2*, 1484.
[30] C. H. Ke, N. Pugno, B. Peng, H. D. Espinosa, *J. Mech. Phys. Solids* **2005**, *53*, 1314.
[31] M. F. Yu, O. Lourie, M. J. Dyer, K. Moloni, T. F. Kelly, R. S. Ruoff, *Science* **2000**, *287*, 637.
[32] This statement is supported by the fact that the measured total projected length of the delaminated SWNT bundle from the HRSEM images, which includes the segment attached to the other fixed–fixed SWNT bundle, is almost unchanged during the whole peeling experiment.
[33] R. M. Tromp, A. Afzali, M. Freitag, D. B. Mitzi, Z. Chen, *Nano Lett.* **2008**, *8*, 469.
[34] M. Zheng, A. Jagota, E. D. Semke, B. A. Diner, R. S. Mclean, S. R. Lustig, R. E. Richardson, N. G. Tassi, *Nat. Mater.* **2003**, *2*, 338.
[35] Y. Mikata, *Acta Mech.* **2007**, *190*, 133.
[36] M. R. Falvo, G. J. Clary, R. M. Taylor, V. Chi, F. P. Brooks, S. Washburn, R. Superfine, *Nature* **1997**, *389*, 582.
[37] O. A. Goussev, P. Richner, U. W. Suter, *J. Adhes.* **1999**, *69*, 1.
[38] L. D. Landau, E. M. Lifshitz, *Theory of Elasticity*, Pergamon Press, Oxford **1986**.
[39] D. W. Nicholson, *Int. J. Fract.* **1977**, *13*, 279.
[40] K. Kendall, *J. Adhes.* **1973**, *5*, 105.
[41] J. Peng, J. Wu, K. C. Hwang, J. Song, Y. Huang, *J. Mech. Phys. Solids* **2008**, *56*, 2213.
[42] J. Wu, K. C. Hwang, Y. Huang, *J. Mech. Phys. Solids* **2008**, *56*, 279.
[43] Y. Huang, J. Wu, K. C. Hwang, *Phys. Rev. B* **2006**, *74*, 245413.
[44] M. M. J. Treacy, T. W. Ebbesen, J. M. Gibson, *Nature* **1996**, *381*, 678.
[45] R. Saito, G. Dresselhaus, M. S. Dresselhaus, *Physical Properties of Carbon Nanotubes*, Imperial College Press, London **1998**.
[46] J. P. Lu, *Phys. Rev. Lett.* **1997**, *79*, 1297.
[47] L. A. Girifalco, M. Hodak, R. S. Lee, *Phys. Rev. B* **2000**, *62*, 13104.
[48] A. Thess, R. Lee, P. Nikolaev, H. J. Dai, P. Petit, J. Robert, C. H. Xu, Y. H. Lee, S. G. Kim, A. G. Rinzler, D. T. Colbert, G. E. Scuseria, D. Tomanek, J. E. Fischer, R. E. Smalley, *Science* **1996**, *273*, 483.
[49] J. E. Lennard-Jones, *Proc. R. Soc. London Ser. A* **1930**, *129*, 598.

Received: September 24, 2009
Published online: December 8, 2009

